Inorganic Chemistry

Article

pubs.acs.org/IC

Spin-State Ordering in Hydroxo-Bridged Diiron(III)bisporphyrin Complexes

Mala A. Sainna,[†] Debangsu Sil,[‡] Dipankar Sahoo,[‡] Bodo Martin,[§] Sankar Prasad Rath,*[,‡] Peter Comba,*[,§] and Sam P. de Visser*[,†]

[†]Manchester Institute of Biotechnology and School of Chemical Engineering and Analytical Science, The University of Manchester, 131 Princess Street, Manchester M1 7DN, United Kingdom

[‡]Department of Chemistry, Indian Institute of Technology Kanpur, Kanpur 208016, India

[§]Anorganisch-Chemisches Institüt and Interdisciplinary Center for Scientific Computing (IWR), University of Heidelberg, Im Neuenheimer Feld 270, 69120 Heidelberg, Germany

Supporting Information

ABSTRACT: We report the synthesis, structure, and spectroscopic characterization of 1,2-bis[μ-hydroxo iron(III) 5-(2,3,7,8,12,13,17,18-octaethylporphyrinyl)]ethane with PF_6^- and SbF_6^- counteranions. The two iron centers are non-equivalent with admixed intermediate spin state ($S = {}^3/_2$ with a minor contribution of $S = {}^5/_2$) on each metal both in the solid and in solution. The molecules are compared with previously known μ-hydroxo complexes with other counterions, such as I_3^-, BF_4^-, and ClO_4^-, which demonstrates that the nature of the counterion can affect the spin-state ordering dramatically. To understand how the spin-state ordering is affected by external perturbations, we also have done a comprehensive computational study. The calculations show that subtle environmental perturbations affect the spin-state ordering and relative energies and are likely to be the root cause of the variation in spin-state ordering observed experimentally.

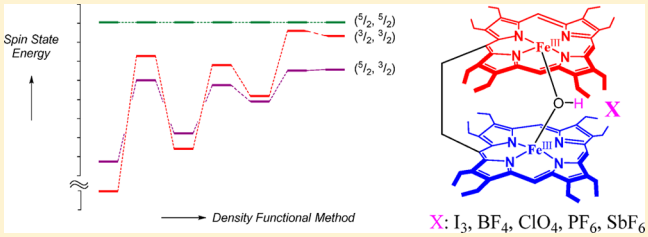

INTRODUCTION

Spin-state ordering is an important feature in transition metal catalyzed reactions in biology as well as in synthetic models, where the spin state of the reactant often determines the catalytic efficiency of the system. Nature often uses transition metals as catalytic reaction centers in enzymes, and metal centers are also used as electron-transfer complexes. In many of these systems the active center has two (or more) interacting metal ions, which often are iron atoms. Examples of diiron-containing enzymes and proteins include hemerythrin,[1] ribonucleotide reductase (RNR),[2] ferritin,[3] methane monoxygenase (MMO),[4] and Δ^9-stearoyl-acyl carrier protein desaturase,[5] to name a few well-studied systems. These diiron enzymes have diverse functions in biology, and all have the two iron ions separated by ~3−5 Å and linked to the protein via nonheme interactions with histidine and carboxylate (Glu/Asp) residues. Hemerythrin and ferritin are proteins involved in oxygen transport and iron storage, whereas other diiron enzymes, such as RNR, catalyze the biosynthesis of deoxyribonucleotides from ribonucleotides. MMO is one of the most efficient biochemical oxidants in nature and one of the few enzymes that can hydroxylate methane.

In contrast to these nonheme diiron proteins, cytochrome c oxidase (C*c*O) has a central dimetal complex, where one of the metals binds to a heme group, and the other is in a nonheme environment. C*c*O is a trans-membrane protein that reduces molecular oxygen to water and thereby releases four electrons that are shuttled through the membrane.[6] To enable oxygen reduction it has a specific active site structure with two metal centers in close proximity. The intricate details of dioxygen binding and reduction as well as the electronic and spin-state coupling between the two metal centers in dimetal proteins, such as C*c*O, are still shrouded in mysteries. To gain insight into spin-state interactions between metal centers, synthetic analogues have been created that model the enzymatic systems.[6b,7] These studies have given insight into the electronic and spectroscopic properties of short-lived intermediates in the catalytic cycle of C*c*O and other dimetal enzyme centers.

In several diiron enzymes, such as MMO and RNR, catalytic intermediates have been proposed with an oxo, peroxo, or hydroxo group bridging the two iron centers, frequently in conjunction with a bridging carboxylate group.[8] The spin multiplicity on each of the metal centers has an effect on the overall reaction mechanism and may vary during the catalytic cycle. Thus, in many metal-catalyzed reactions a multistate reactivity pattern has been established on low-lying electronic and spin states.[9] For instance, computational modeling established a degenerate pair of doublet and quartet spin states for the active oxidant of cytochrome P450, that is, compound I.[10] It was found that in each of these spin states the oxidant can react

Received: November 24, 2014
Published: January 22, 2015

DOI: 10.1021/ic502803b
Inorg. Chem. 2015, 54, 1919−1930

with a substrate to form products with different rate constants and sometimes even different mechanisms. Understanding the factors that contribute to spin-state ordering and relative energies in transition metal complexes, therefore, is important and may affect reactivity patterns.

Oxo- and hydroxo-bridged diiron active centers are common structural motifs found among proteins involved in O_2 metabolism. The transformation of an oxo to a hydroxo bridge is a proposed step in the reaction pathways of a great variety of iron and copper redox enzymes. As enzymatic systems are difficult to study experimentally, synthetic model complexes have been developed that contain the characteristic features of enzyme active sites. Recently, we reported the spectroscopic characterization of a series of 1,2-bis[μ-hydroxo iron(III) 5-(2,3,7,8,12,13,17,18-octaethylporphyrinyl)]ethane complexes, **1b**·X (Scheme 1; X = I_3^-, BF_4^-, and ClO_4^-), in which the two

Scheme 1. Structures Investigated in This Work

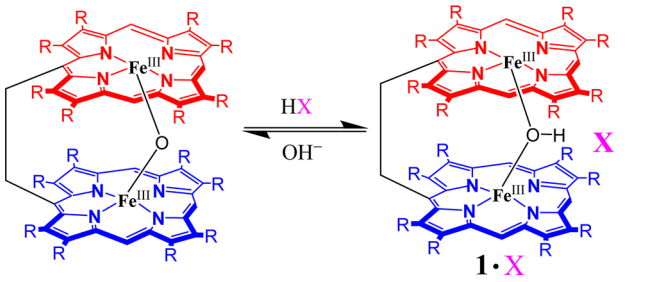

X: I_3, BF_4, ClO_4, PF_6, SbF_6

1a: R = H

1b: R = C_2H_5

iron(III) centers are either equivalent or nonequivalent based on the counteranions present, although both cores have identical molecular structures.[11] All complexes were crystallographically characterized and showed considerable doming of both porphyrin cores and out-of-plane displacement of the metal ions. Also, the spin states were found to be dependent on the counterions used. In particular, spectroscopic investigation of **1b**·I_3 identified core I (shown in red in Scheme 1) as having nearly high-spin configuration ($S = {}^5/_2$ with a minor contribution of $S = {}^3/_2$), whereas core II (shown in blue in Scheme 1) had an admixed intermediate spin state ($S = {}^3/_2$ with a minor contribution of $S = {}^5/_2$) both in the solid and solution phases.[11] Complex **1b**·BF_4 was, however, found to have two iron(III) centers with admixed intermediate states, whereas **1b**·ClO_4 was characterized to have high-spin ($S = {}^5/_2$) iron(III) centers in the solid but nearly intermediate ($S = {}^3/_2$) spin in solution. It appears, therefore, that changing the counterion affects the spin-state ordering and spin coupling between the two iron centers. Dependence of the spin states of the metal complexes on counteranions has been found rarely, particularly with anions that are far away and not apparently involved in a direct interaction with the metal site.[11−13] How counteranions affect the spin-state ordering and coupling of metal centers is currently unknown, which encouraged us to do a further study, where we combined experiment with computation.

In the present work, counteranions such as PF_6^- and SbF_6^- were used that are octahedral in geometry and nearly spherical in shape. The synthesis, structure, and properties of the corresponding μ-hydroxo diiron(III)bisporphyrin complexes are reported here and compared with similar complexes reported before. The ethyl linker, which bridges two porphyrin rings, introduces significant horizontal and vertical flexibility to the bisporphyrin framework and also brings the two porphyrin moieties close enough to distort the macrocycles significantly in the μ-hydroxo complexes.

EXPERIMENTAL METHODS

Synthesis. The μ-oxo diiron(III)bisporphyrin was prepared using procedures reported previously.[14] Reagents and solvents were purchased from commercial sources and purified by standard procedures before use.

***1b*·PF_6.** The μ-oxo diiron(III)bisporphyrin (100 mg, 0.082 mmol) was dissolved in 100 mL of dichloromethane, and 100 mL of 5% HPF_6 (aqueous) solution was added to it and stirred for 15 min. The organic layer was separated and dried over anhydrous Na_2SO_4, and the solution was evaporated to complete dryness. The solid product was dissolved in a minimum volume of CH_2Cl_2 and then carefully layered with *n*-hexane and allowed to undergo slow diffusion in air at room temperature. After standing for 7−8 d in air, purple crystalline material of the title complex were separated out and dried in vacuum. Yield: 92 mg (82%). UV−vis (dichloromethane) [λ_{max}, nm (ε, M^{-1} cm^{-1})]: 375 (1.3×10^5), 632 (4.6×10^3). ^{1}H NMR ($CDCl_3$, 295 K): *meso*-H: −1.0, −3.9, −11.9, −15.6; $-CH_3$: 2.7, 2.8, 2.9, 3.3, 3.4; CH_2: 14.0, 15.0, 15.5, 16.0, 16.7, 17.0, 17.2, 18.1, 18.2, 18.7, 19.3, 21.3, 21.6, 21.9, 22.7, 28.3; CH_2 (b): 31.9, 33.7 ppm.

***1b*·SbF_6.** The μ-oxo diiron(III)bisporphyrin (100 mg, 0.082 mmol) was dissolved in 100 mL of dichloromethane, and 100 mL of 5% $HSbF_6$ (aqueous) solution was added to it and stirred for 15 min. The organic layer was separated and dried over anhydrous Na_2SO_4, and the solution was evaporated to dryness. The solid product was dissolved in a minimum volume of benzene, which was then carefully layered with *n*-hexane, after which the volatiles were allowed to undergo slow diffusion in air at room temperature. After standing for 7−8 d in air, purple crystalline materials of the complex were separated out and dried in high vacuum. Yield: 89 mg (75%). UV−vis (dichloromethane) [λ_{max}, nm (ε, M^{-1} cm^{-1})]: 376 (1.8×10^5), 639 (4.4×10^3). ^{1}H NMR ($CDCl_3$, 295 K): *meso*-H: −1.0, −3.9, −11.9, −15.7; $-CH_3$: 2.6, 2.8, 2.9, 3.3, 3.4; CH_2: 14.2, 15.2, 15.7, 16.0, 16.7, 17.2, 18.0, 18.2, 18.7, 19.3, 21.5, 22.1, 23.0, 28.5; CH_2 (b): 31.9, 33.8 ppm.

Instrumentation. UV−vis spectra were recorded on a PerkinElmer UV−visible spectrometer. Elemental (C, H, and N) analysis was performed on a PerkinElmer 2400II elemental analyzer. ^{1}H NMR spectra were recorded on a JEOL 500 MHz instrument. The spectra for paramagnetic molecules were recorded over a 100 kHz bandwidth with 64 K data points and a 5 ms 90° pulse. For a typical spectrum, between 2000 and 3000 transients were accumulated with a 50 μs delay time. The residual ^{1}H resonances of the solvents were used as a secondary reference. ^{57}Fe Mössbauer spectra were recorded using a Wissel 1200 spectrometer and a proportional counter. ^{57}Co(Rh) in a constant acceleration mode was used as the radioactive source. Isomer shifts (δ) are given relative to α-iron foil at room temperature. Magnetic susceptibility data were collected using a Quantum Design MPMS SQUID magnetometer over the temperature range from 5 to 300 K.

X-ray Structure Solution and Refinement. Single-crystal X-ray data of **1b**·SbF_6 were collected at 100 K on a Bruker SMART APEX CCD diffractometer equipped with CRYO Industries low-temperature apparatus, and intensity data were collected using graphite-monochromated Mo Kα radiation (λ = 0.710 73 Å). The data integration and reduction were processed with SAINT software.[15] An absorption correction was applied,[16] and the structure was solved by the direct method using SHELXS-97 and was refined on F^2 by full-matrix least-squares technique using the SHELXL-2014 program package.[17] Non-hydrogen atoms were refined anisotropically. The proton of the hydroxo bridge was directly located in the difference Fourier maps, while the other hydrogen atoms were included in calculated positions. In the refinement, hydrogens were treated as riding atoms using SHELXL default parameters. Crystallographic data and data collection parameters are given in Table S1 (see Supporting Information).

DOI: 10.1021/ic502803b
Inorg. Chem. 2015, 54, 1919−1930

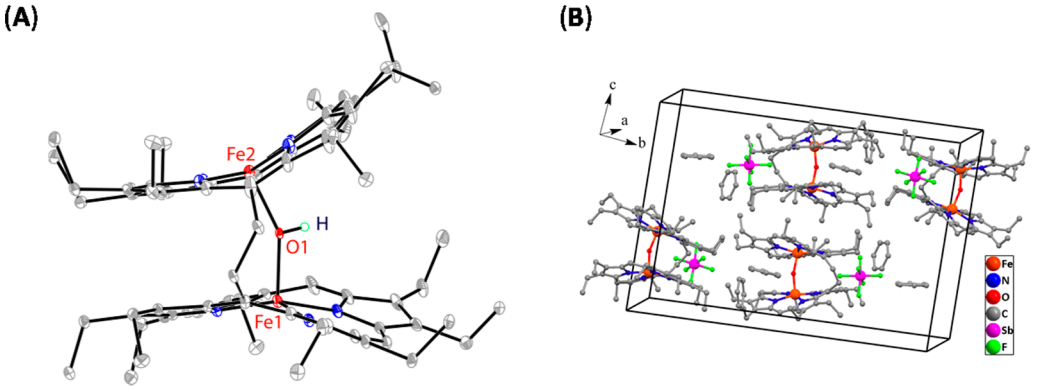

Figure 1. (A) A perspective view of **1b**·SbF_6 (without C_6H_6 and SbF_6^- counteranion) showing 50% thermal contours for all non-hydrogen atoms at 100 K (all hydrogen atoms except for the μ-hydroxo proton were omitted for clarity). (B) Diagram illustrating the packing of **1b**·SbF_6·C_6H_6.

Computational Methods and Procedures. The work described here is focused on the computational description of μ-hydroxo diiron(III)bisporphyrin **1**·X with particular focus on the spin-state ordering and relative energies. Because of the size of the system, some of the calculations were done on the full model (with ethyl side chains on both porphyrin rings), **1b**, whereas other calculations use an abbreviated model with all side chains replaced by hydrogen atoms, **1a**. The initial work was done on the crystal structure coordinates of the μ-hydroxo-diiron(III)bisporphyrin **1b**·I_3 with the counteranion removed, Scheme 1, with a total of 176 atoms and overall charge +1. Data was benchmarked against the data from ref 11, using a range of density functional theory (DFT) methods and basis sets and initially focused on the spin-state ordering and energies.

Technically, a bridged μ-hydroxo diiron(III)bisporphyrin can exist in three possible spin configurations on each metal center that is either ferromagnetically or antiferromagnetically coupled. As such, there are a large number of possible spin−spin interactions between the metal centers of which we took a representative sample. Experimental studies on **1b**·I_3 indicate a spin multiplicity of $S = {}^5/_2$ on the iron center of core I and a gross multiplicity of ${}^3/_2$ on the iron center of core II.[11] In a first set of calculations we took the crystal structure coordinates of **1b**·I_3. As we were interested in the free energy differences of the various spin states we attempted a frequency calculation on this structure. However, as the coordinates were taken from the crystal structure, this had a large number of imaginary frequencies. We therefore ran a subsequent constraint geometry optimization, whereby the coordinates of all ethyl side chains were minimized and the porphyrin cores were kept fixed. This gave a frequency calculation with few imaginary frequencies.

Structure **1b**·I_3 was calculated (without I_3^- counterion) with an overall charge of +1 and total spin multiplicities of S_{tot} (core I, core II) = 5 (${}^5/_2$, ${}^5/_2$), 4 (${}^5/_2$, ${}^3/_2$), 3 (${}^3/_2$, ${}^3/_2$), and 1 (1/2, 1/2). All calculations were performed using the GAUSSIAN-09 suite of programs[18] exploiting unrestricted DFT methods with a variety of hybrid and nonhybrid exchange-correlation functionals: B3LYP,[19] B3LYP* (i.e., B3LYP with 15% HF exchange),[20] BP86,[21] OLYP,[22] OPBE,[23] and TPSSh.[24]

We tested three different basis set combinations labeled as BS1, BS2, and BS3. All initial studies were done with a modest double-ζ quality basis set on iron that contains an effective core potential (LANL2DZ), in combination with a 6-31G basis set on the remaining atoms: BS1.[25] This basis set was chosen to reduce computational cost as well as used as a comparison with a mixed-valent basis set of triple-ζ quality consisting of DEF2-TZVP[26] on iron and the four nitrogen ligands in the first coordination sphere of each of the porphyrin rings, whereas the remaining atoms were calculated using a 6-31G basis set: BS2. Finally, the atoms of the complete complex **1b** were also calculated with the triple-ζ quality basis set DEF2-TZVP throughout: BS3. The system was calculated with each of the basis sets BS1, BS2, and BS3 coupled to all the density functional methods outlined above and the energetics were tabulated for comparison.

In a final set of calculations, we ran several full-geometry optimizations whereby the counteranion was included. Calculations were performed on **1b**·X and **1a**·X, with X = I_3^-, BF_4^-, or ClO_4^-, whereby all degrees of freedom were minimized. These calculations were run in Jaguar[27] at the B3LYP/BS1 level of theory.

To understand the differences in spin-state ordering between the individual porphyrin cores, we also split structure **1b**·I_3 into individual cores, whereby each monomer was capped with a hydrogen atom at the trimmed ethyl bridge and each of the separate cores were calculated using the same BS1, BS2, and BS3 basis sets together with the chosen density functional method. In these monomer units, we tested OH^- and H_2O as the distal ligand mimicking the bridged μ-hydroxo group in structure **1b**·I_3. The two separated monoporphyrins were also capped with methoxy (CH_3O^-) or methanol (CH_3OH) in place of OH^- and H_2O, respectively, because they may be geometrically closer to the actual conformation in **1b**·I_3.

RESULTS AND DISCUSSION

Synthesis. The synthesis of the μ-oxo bridged diiron(III)-bisporphyrin was reported earlier.[14a,b] Diiron(III)-μ-hydroxo complexes were prepared in a mixed phase reaction by treatment of the μ-oxo bridged diiron(III)bisporphyrin upon protonation by a strong Brønsted acid with weakly coordinating counteranions.[11] During the process, the green color of the oxo-bridged dimer changed to red. Brønsted acids used in the present work are HPF_6 and $HSbF_6$, which eventually produce the corresponding μ-hydroxo complex **1b**·X, where X = PF_6^- or SbF_6^-, respectively. When dichloromethane solution of the μ-hydroxo complex is treated with aqueous NaOH, the μ-oxo complex is formed, which can be converted again to the starting μ-hydroxo complex just upon protonation. The clean conversion is completely reversible and rapid with a sharp change in color as studied by UV−vis and ^{1}H NMR. Scheme 1 shows the synthetic outline of complexes along with their abbreviations used here. While **1b**·I_3, **1b**·BF_4, and **1b**·ClO_4 have been reported earlier,[11] the data for **1b**·PF_6 and **1b**·SbF_6 are presented here. The complexes were isolated as crystalline solids in good yields, and **1b**·SbF_6 was structurally characterized. The solid-state structures are also preserved in solution as reflected in the ^{1}H NMR spectra in $CDCl_3$ (vide infra).

Crystallographic Characterization of 1b·SbF_6. Crystals suitable for X-ray diffraction were grown by slow diffusion of *n*-hexane into a benzene solution of **1b**·SbF_6 at room temperature under air. The molecule crystallizes in the monoclinic crystal system with $P2_1/c$ space group. A perspective view of the molecule is shown in Figure 1, while selected bond distances and angles are given in Table 1. The proton of the μ-hydroxo bridge was directly located in the difference Fourier map with an O−H length of 0.78(2) Å. The two Fe−O(H) distances are 1.933(4)

DOI: 10.1021/ic502803b
Inorg. Chem. 2015, 54, 1919−1930

Table 1. Selected Bond Lengths (Å) and Bond Angles (deg) in 1b·SbF$_6$

Fe1−O1	1.933(4)
Fe1−N1	1.973(5)
Fe1−N2	1.983(5)
Fe1−N3	1.968(5)
Fe1−N4	1.981(5)
Fe2−O1	1.940(4)
Fe2−N101	1.978(5)
Fe2−N102	1.972(4)
Fe2−N103	1.965(5)
Fe2−N104	1.965(5)
C37−C38	1.573(13)
Fe1−O1−Fe2	152.11(19)
O1−Fe1−N1	95.75(18)
O1−Fe1−N2	98.90(18)
O1−Fe1−N3	100.08(19)
O1−Fe1−N4	99.01(18)
O1−Fe2−N101	102.24(18)
O1−Fe2−N102	99.78(18)
O1−Fe2−N103	96.01(19)
O1−Fe2−N104	96.2(2)

and 1.940(4) Å, which are much longer than that of the Fe−O distance of the μ-oxo dimer.[14] The average Fe−N$_p$ bond lengths for the two porphyrin cores are 1.976(5) and 1.970(5) Å, and the out-of-plane displacements of iron from the mean plane of the C$_{20}$N$_4$ porphyrinato core (Fe···Ct$_p$) is 0.35 Å. These values are lowest among all other μ-hydroxo species reported so far, using the same ethane-bridged bisporphyrin framework. The Fe−O−Fe angle is 152.11(19)°, and the Fe···Fe nonbonding distance is 3.759(1) Å. The average displacement of atoms from the mean plane of the C$_{20}$N$_4$ porphyrinato core is 0.26 and 0.29 Å for core I and core II, respectively. The relative orientation of the two porphyrin rings gives an interplanar angle of 24.8°. The counteranion SbF_6^- remains at a long distance from the two iron centers of the molecule. The packing diagram of the molecule is shown in Figure 1B.

Five-coordinate iron(III) porphyrins can exist as high-spin ($S = {}^5/_2$), intermediate-spin ($S = {}^3/_2$), and also as quantum mechanical spin admixed states with varying proportions of pure $S = {}^3/_2$ and $S = {}^5/_2$ states.[28] When the energy separation of the intermediate-spin and high-spin states approaches the magnitude of the spin−orbit coupling parameter, the electronic ground state of the heme is best described as a quantum mechanical admixture of the two spin states. The structural parameters, important for identifying the spin state, are the displacement of the iron from the mean plane of the C$_{20}$N$_4$ porphyrinato core (Fe···Ct$_p$) and the average Fe−N$_p$ distance.[28,31] For the five-coordinate high-spin case, the typical Fe−N$_p$ and Fe···Ct$_p$ distances are ≥2.045 and ≥0.42 Å, respectively. On the other hand, values reported for five-coordinate spin-admixed iron(III) porphyrinates are in the range of 1.961−2.038 Å for Fe−N$_p$ and 0.10−0.36 Å for Fe···Ct$_p$, which vary according to the amount of $S = {}^3/_2$, ${}^5/_2$ character present in the porphyrin core. For **1b**·SbF$_6$, however, the average Fe−N$_p$ bond lengths for the two porphyrin cores are 1.976(5) and 1.970(5) Å, while Fe···Ct$_p$ is 0.35 Å. These values are characteristic for admixed intermediate spin ($S = {}^3/_2$ with only a minor contribution of $S = {}^5/_2$) of iron present in the molecule.

The salient structural features of the μ-hydroxo cation of **1b**·SbF$_6$ isolated from independent determination are compared with their corresponding μ-oxo dimer and also with **1b**·I$_3$, **1b**·BF$_4$, and **1b**·ClO$_4$ in Table 2. The corresponding μ-oxo diiron(III)bisporphyrin crystallizes as two different solvates that are grown from two different solvent combinations; however, both of them have very similar structures and geometrical parameters.[14a,b] Upon protonation, the Fe−O distance increases, although the Fe−O(H)−Fe unit remains almost unchanged in **1b**·SbF$_6$, while with other μ-hydroxo complexes reported earlier the unit is considerably bent.[11] The Fe···Fe distances, upon protonation, are also increased. The average Fe−N$_p$ distance and displacement of the metal from the mean porphyrin plane (Fe···Ct$_p$) in **1b**·SbF$_6$ are, however, shortest in the series and are similar to the values typically observed in the five-coordinate iron(III)porphyrins with admixed intermediate-spin state. In contrast, **1b**·I$_3$ was assigned to nearly high-spin and admixed intermediate-spin states of Fe in cores I and II, respectively, while two admixed intermediate spins are present in **1b**·BF$_4$. Moreover, the two iron centers in **1b**·ClO$_4$ are equivalent and are assigned to be high-spin in solid.

The porphyrin rings are highly distorted in **1b**·SbF$_6$. In particular, the meso carbons that are connected through the bridging ligand are strongly displaced. Figure 2 compares the out-of-plane displacements (in units of 0.01 Å) of the porphyrin core atoms of **1b**·SbF$_6$ with previously reported **1b**·I$_3$ and **1b**·BF$_4$. As can be seen, the porphyrin ring distortions of **1b**·SbF$_6$ can be described mostly as ruffled, and the two porphyrin cores are significantly deformed but to an unequal extent, which consequently makes them inequivalent (vide infra). Also, the ring deformations of **1b**·SbF$_6$ are similar to those of **1b**·BF$_4$ and thus results a similar spin description for both the complexes.

Table 2. Selected Structural Parameters of 1b·X and Related Complexes

	μ-oxo dimer		**1b**·I$_3$		**1b**·BF$_4$		**1b**·SbF$_6$		**1b**·ClO$_4$	
	core-I	core-II	core-I	core-II	core-I	core-II	core-I	core-II	core-I	core-II
Fe−O [Å]	1.779(2)	1.768(2)	1.897(3)	1.934(3)	1.925(3)	1.967(3)	1.933(4)	1.940(4)	1.911(2)	1.922(2)
Fe−N$_p$ [Å][a]	2.068(3)	2.072(3)	2.051(4)	2.007(4)	2.019(4)	1.967(3)	1.976(5)	1.970(5)	2.063(3)	2.054(3)
Fe−O−Fe [deg]	147.9(1)		142.5(2)		148.5(2)		152.11(19)		141.2(1)	
Δ^{Fe}_{24} [Å][b]	0.55	0.60	0.55	0.48	0.41	0.39	0.35	0.35	0.57	0.48
Fe···Fe [Å]	3.409(1)		3.627(1)		3.747(1)		3.759(1)		3.615(1)	
interplanar angle [deg][c]	25		29.5		26.7		24.8		27.8	
Δ_{24} [Å][d]	0.21	0.20	0.21	0.31	0.22	0.31	0.26	0.29	0.17	0.13
twist angle [deg][e]	16.1		12.88		14.85		16.3		10.85	

[a]Average value. [b]Displacement of iron from least-squares plane of C$_{20}$N$_4$ porphyrinato core. [c]Angle between two least-squares plane of C$_{20}$N$_4$ porphyrinato core. [d]Average displacement of atoms from the least-squares plane of C$_{20}$N$_4$ porphyrinato core. [e]Average value of four N−Fe−Fe′−N′ dihedral angles.

DOI: 10.1021/ic502803b
Inorg. Chem. 2015, 54, 1919−1930

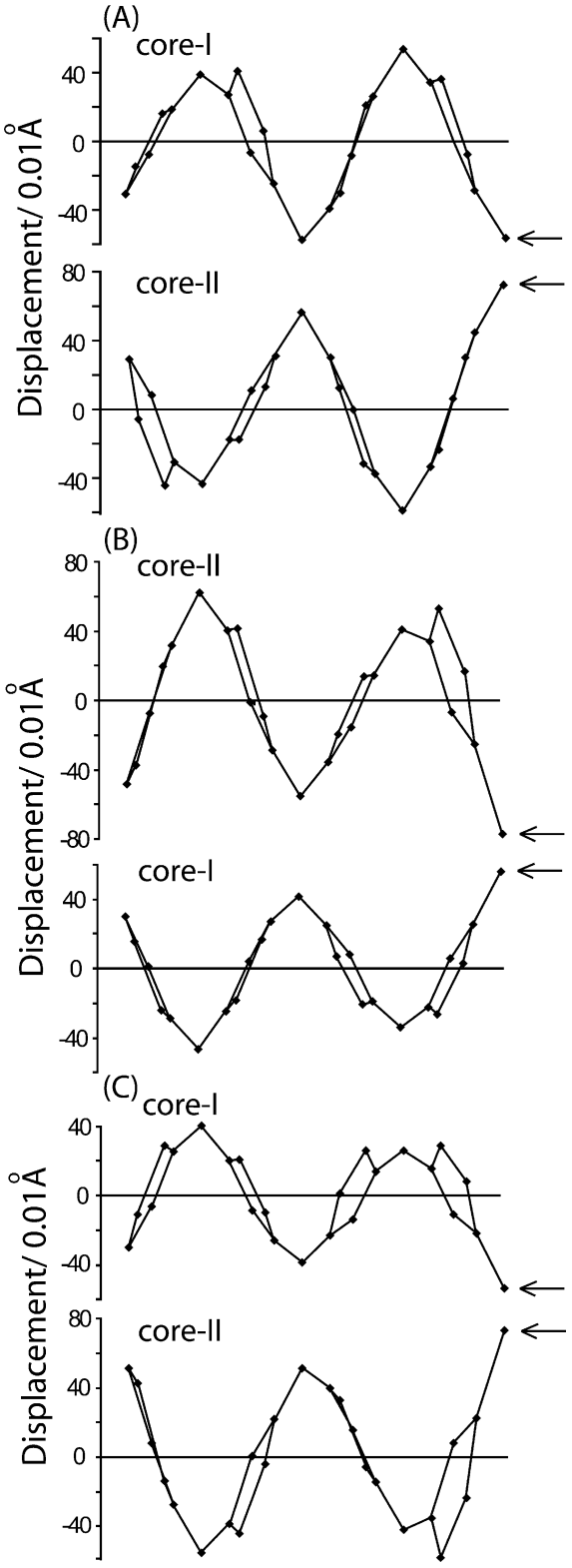

Figure 2. Atom deviations (in units of 0.01 Å) from the least-squares plane of the $C_{20}N_4$ porphyrinato core of (A) **1b**·SbF_6, (B) **1b**·BF_4, and (C) **1b**·I_3. The horizontal axis represents the atom number in the macrocycle showing the bond connectivity between atoms, and the arrows show the bridging meso carbons.

Mössbauer Spectroscopy. Mössbauer parameters are among the most powerful probes to determine the spin states in iron(III) porphyrin complexes.[28,29] While the isomer shift (δ) values of the high-spin and intermediate-spin states are quite similar (0.5−0.3 mm s^{-1}), the quadrupole splitting (ΔE_Q) values are very much different, namely, ≤1.0 and ≥3.0 mm s^{-1} for the high-spin and intermediate-spin complexes, respectively. Mössbauer spectra of polycrystalline samples of **1b**·PF_6 and **1b**·SbF_6 were recorded in the absence of an applied magnetic field at room temperature. The isomer shifts of **1b**·PF_6 and **1b**·SbF_6 appear in the range from 0.2 to 0.3 mm s^{-1} which are typical for pentacoordinate ferric sites with O coordination.[12,28,29] The μ-oxo diiron(III)bisporphyrin shows small quadrupole splitting [δ (ΔE_Q): 0.28 (0.61) mm s^{-1}] characteristic of the high-spin iron(III).[13a] The previously reported μ-hydroxo bridged diiron(III)bisporphyrin **1b**·I_3 shows two quadrupole split doublets [δ (ΔE_Q) mm s^{-1}: 0.28 (1.16) and 0.29 (2.35)], which correspond to two inequivalent iron(III) centers, one with nearly high-spin ($S = {}^5/_2$ with minor contribution of $S = {}^3/_2$) and the other with admixed intermediate-spin.[11] Another reported μ-hydroxo bridged diiron(III)bisporphyrin **1b**·BF_4 also shows two quadrupole split doublets [δ (ΔE_Q) mm s^{-1}: 0.25 (1.55), 0.27 (2.85)] at the same temperature, consistent with two different admixed intermediate-spins of Fe.[11a] In the present case both **1b**·PF_6 and **1b**·SbF_6 also show two quadrupole split doublets; for **1b**·PF_6, δ (ΔE_Q), mm s^{-1}: 0.25 (2.99), 0.22 (2.09), and for **1b**·SbF_6, δ (ΔE_Q), mm s^{-1}: 0.28 (2.95), 0.25 (2.10). Therefore, the iron centers in these complexes are assigned to have two admixed intermediate-spin states ($S = {}^3/_2$ with only a small contribution from $S = {}^5/_2$). Figure 3 shows Mössbauer spectra of the μ-hydroxo complexes reported here with two clear quadrupole split doublets. It is interesting to note here that Mössbauer spectra of **1b**·ClO_4 and $\{[Fe^{III}(OEP)]_2(OH)\}ClO_4$, OEP = octaethylporphyrin, show only one quadrupole split doublet δ (ΔE_Q): 0.26(1.09) and 0.40 (1.13) mm s^{-1}, respectively, and the corresponding iron centers were thus assigned to be high-spin in nature.[11a,29a] Moreover, large single quadrupole splitting in the Mössbauer spectra of $\{[Fe(TPP)]_2(OH)\}[CB_{11}H_6Cl_6]$ and $\{[Fe(TPP)]_2(OH)\}[F_{20}\text{-}BPh_4]$ (ΔE_Q = 3.29, 1.8 mm s^{-1}, respectively), TPP = tetraphenylporphyrin, at room temperature, identify two equivalent iron centers with admixed intermediate ($S = {}^3/_2, {}^5/_2$) state.[30]

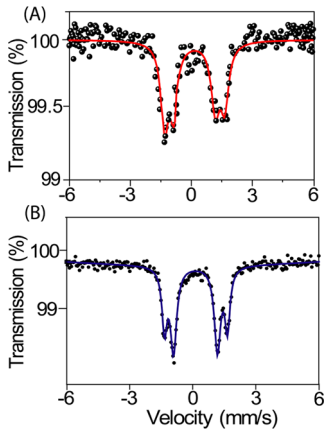

Figure 3. Zero-field Mössbauer spectra of polycrystalline samples of (A) **1b**·SbF_6 and (B) **1b**·PF_6 at 298 K.

^{1}H NMR Spectroscopy. The solution structure and properties of the complexes can be obtained from their ^{1}H NMR spectra in $CDCl_3$ (at 295 K). The ^{1}H NMR resonance patterns of the complexes should be similar to those of meso-substituted five-coordinate iron(III) porphyrins of type

DOI: 10.1021/ic502803b
Inorg. Chem. 2015, 54, 1919−1930

[Fe^{III}(*meso*-R-OEP)X], R = alkyl and X = halide, provided that the two porphyrin moieties in the molecule are equivalent. It is therefore expected that each porphyrin core should provide two meso resonances in a 2:1 intensity ratio, namely, eight methylene and four equally intense methyl resonances. The eight methylene resonances arise due to the diastereotopic nature of these protons as a result of inequivalency of the two sides of the porphyrin ring.[31] Resonance assignments are made based on the relative intensities and line widths of the peaks as well as on the basis of a ^{1}H−^{1}H COSY experiment.

Figure 4 shows the ^{1}H NMR spectra of **1b**·SbF_6 in $CDCl_3$ at 295 K. Here, the presence of 16 sharp ethylene proton signals in

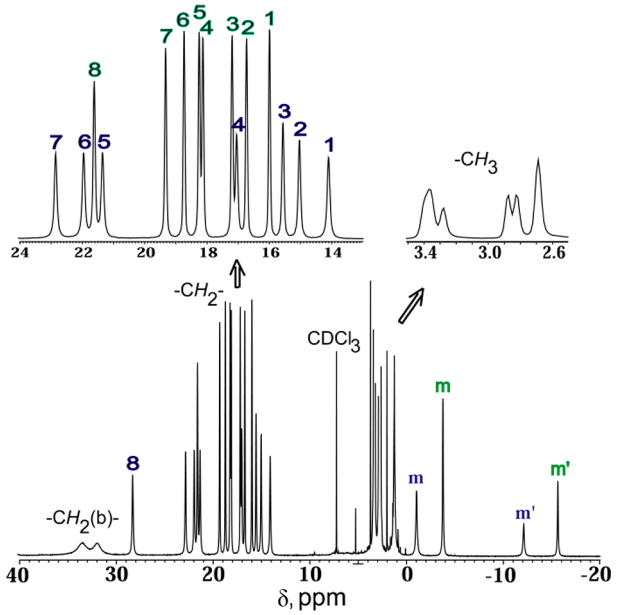

Figure 4. ^{1}H NMR spectra in $CDCl_3$ at 295 K for **1b**·SbF_6.

the narrow range from 28.5 to 14.2 ppm and four sharp meso signals (at −1.0, −3.9, −11.9, −15.7 ppm) demonstrate the presence of two inequivalent Fe centers in the molecule that can be clearly visible in two distinct sets of signals (one set is numbered in blue; the other in green). Two broad peaks for the bridging methylene protons are observed at 31.9 and 33.8 ppm. The ^{1}H NMR chemical shifts of methylene and meso hydrogen atoms are highly sensitive to the spin states of the iron center. The position of the methylene and meso proton signals of **1b**·SbF_6 is very similar to what has been observed for **1b**·BF_4. On the basis of the above results, the spin states of the Fe in **1b**·SbF_6 can be assigned to two admixed intermediate spins ($S = {}^3/_2$ with only a small contribution from $S = {}^5/_2$) of iron, as also observed in the solid phase. These features in the spectrum authenticate two inequivalent porphyrin iron centers in the molecule. The ^{1}H NMR peak position and pattern for **1b**·PF_6 remains very similar to that of **1b**·SbF_6, which confirms two inequivalent Fe centers with two admixed intermediate-spin configurations of iron in solution.

To compare the ^{1}H NMR spectra of **1b**·SbF_6 with that of the previously reported μ-hydroxo complex **1b**·I_3,[12] we display the two spectra underneath each other in Figure 5. As can be seen in **1b**·I_3, two very distinct sets of signals are observed. In one set, eight methylene signals are relatively broad, spanning from 68.8 to 21.2 ppm, while two broad meso signals arise at −10.3 and −35.5 ppm in a 2:1 intensity ratio, observed due to the nearly

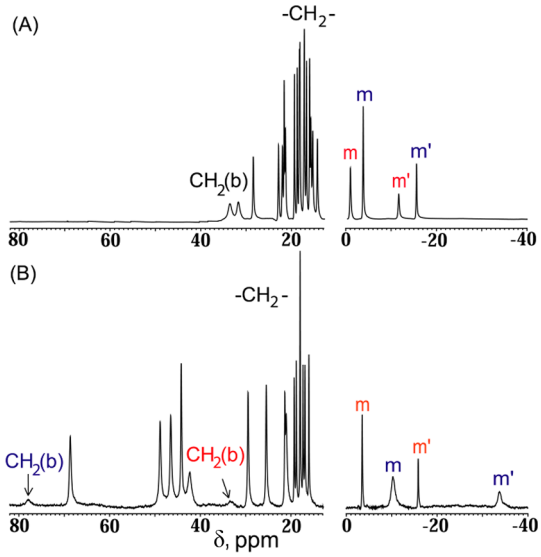

Figure 5. ^{1}H NMR spectra in $CDCl_3$ at 295 K (A) **1b**·SbF_6 for and (B) for **1b**·I_3.

high-spin ($S = {}^5/_2$) nature of iron present in core-I. In the other set, eight sharp methylene peaks appear at a relatively narrow region (from 19.9 to 16.1 ppm), and the two sharp meso resonances in a 2:1 ratio at −3.5 and −15.9 ppm that are due to admixed intermediate spin ($S = {}^3/_2$ with only a small contribution from $S = {}^5/_2$) of iron present in core-II. In contrast, the ^{1}H NMR of **1b**·SbF_6 shows 16 sharp ethylene proton signals in the narrow range of 28.5 to 14.2 ppm as well as four sharp meso signals, which authenticate two inequivalent iron(III) porphyrins with stabilization of two different admixed intermediate-spin states, as also observed in the solid (vide supra). Thus, the spin-state configurations of **1b**·I_3 and **1b**·SbF_6 are found to be dependent on the counteranions.

The Curie plots of the methylene and meso protons for **1b**·SbF_6 are shown in Figure 6. It follows that the average change in

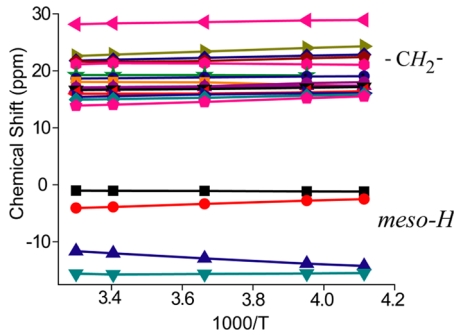

Figure 6. Curie plots of the methylene and meso proton signals of **1b**·SbF_6.

chemical shift of the methylene protons is less than 0.6 ppm over a temperature range from 25 to −40 °C, which implies that the two iron(III) centers are strongly (antiferromagnetically) coupled.[11,12] By contrast, much larger chemical shifts of the methylene groups were found for **1b**·I_3 due to weaker antiferromagnetic coupling between the two iron centers.

The values of the chemical shift for the $-CH_3$ protons of the ethyl substituents are also found to be sensitive to the overall spin state. In particular, the $S = {}^5/_2$ complexes exhibit $-CH_3$ signals in the ^{1}H NMR spectra that are shifted considerably more

DOI: 10.1021/ic502803b
Inorg. Chem. 2015, 54, 1919−1930

downfield than those for the $S = {}^3/_2$ states. This is because the unpaired electrons are partially delocalized over the $-CH_3$ protons through σ-bond interactions in the $S = {}^5/_2$ complexes.[31,32] ^{1}H NMR signals for the $-CH_3$ substituents were located at 2.7, 2.8, and 2.9 ppm for core I and at 3.2 and 3.4 ppm for core II of **1b**·PF_6, whereas the corresponding values for **1b**·SbF_6 are found at 2.6, 2.8, and 2.9 ppm for core I and 3.3 and 3.4 ppm for core II. Therefore, the positions of the methyl resonances further support the spin-state assignment made above. The ^{1}H NMR spectra were also recorded in alternative solvents (such as CD_2Cl_2, benzene-d_6 and acetone-d_6), and very similar spectral patterns were obtained.

Experimentally, there is no observed proton exchange between the μ-oxo and μ-hydroxo species on the ^{1}H NMR time scale. In $CDCl_3$ at 295 K, separate resonances are observed in a mixture of the two species, and the chemical shifts are unchanged from those of a single component. This probably reflects the steric impossibility of close approach of the protonated Fe−O(H)−Fe moiety to the unprotonated Fe−O−Fe group. However, obtaining a pK_a value in a suitable solvent for such measurements (e.g., DMF, DMSO etc.) is complicated by the tendency of such solvents to act as ligands.

Magnetic Properties. Variable-temperature magnetic susceptibility measurements for the crystalline samples of **1b**·PF_6 and **1b**·SbF_6 were carried out in the solid state. The plots of $\chi_M T$ versus T (K) are simulated, as shown in Figure 7, using the expression derived from the spin Hamiltonian (H)[33]

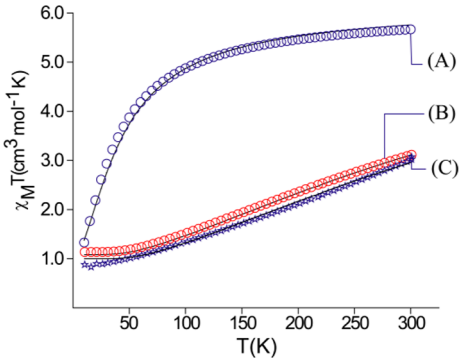

Figure 7. $\chi_M T$ vs T plot for (a) **1b**·I_3, (b) **1b**·PF_6, and (c) **1b**·SbF_6. The solid lines are the best fits using the values given in the text. The g value was fixed at 2.00.

$$H = -2JS_I \cdot S_{II} - \mu \cdot B + D[S_z^2 - \frac{1}{3}S(S+1)] \quad (1)$$

$$\chi_M = (1-p)\frac{Ng^2\beta^2}{kT}\frac{2 + 10e^{4x} + 28e^{10x} + 60e^{18x}}{3 + 5e^{4x} + 7e^{10x} + 9e^{18x}} + 4.375\frac{p}{T} + \mathrm{TIP} \quad (2)$$

where $S_I = {}^5/_2$, $S_{II} = {}^3/_2$, B is the strength of the applied magnetic field, D is the zero-field splitting parameter, $x = (J + D/3)/kT$, p is the mol % of the mononuclear iron(III) impurity, and TIP stands for temperature-independent paramagnetism. The equation yields $J = -37.6 \pm 0.2$ and -36.5 ± 0.2 cm^{-1} for **1b**·PF_6 and **1b**·SbF_6, respectively. Thus, strong antiferromagnetic coupling in the μ-oxo dimer ($J = -126.6$ cm^{-1}) is attenuated to a much weaker exchange interaction in the μ-hydroxo species **1b**·PF_6 and **1b**·SbF_6 reported here.

Two sets of data were collected at the two applied magnetic fields of 0.2 and 1 T and corrected for diamagnetism using Pascal's constant.[34] The data are plotted in $\chi_M T$ versus T for both data sets (Figure 7), which provide very similar fitting parameters. Considering that spin-admixed iron(III) porphyrin complexes have $D \approx 10$ cm^{-1},[35] we took the D values of 10 ± 2 cm^{-1}. From the best fit of eq 2, the parameters obtained for **1b**·PF_6 are $J = -37.6$ cm^{-1}, $p = 1 \times 10^{-7}$ %, and TIP = 7×10^{-5} cm^3 mol^{-1}, and for **1b**·SbF_6, the fitting parameters are $J = -36.5$ cm^{-1}, $p = 0.04$% and TIP = 6×10^{-5} cm^3 mol^{-1}.

Figure 7 compares the $\chi_M T$ versus T plot for **1b**·I_3, **1b**·PF_6 and **1b**·SbF_6, in which the variation of the magnetic behavior between the molecules is evident. The antiferromagnetic coupling between two Fe(III) centers in the μ-hydroxo complex is much stronger in **1b**·PF_6 ($J = -37.6 \pm 0.2$) and **1b**·SbF_6 ($J = -36.5 \pm 0.2$) as compared to **1b**·I_3 with a very small coupling constant of -4.5 cm^{-1}. Further evidence for relatively stronger antiferromagnetic coupling in **1b**·PF_6 and **1b**·SbF_6 comes from the smaller isotropic shifts of the methylene and meso protons (Figure 5) as well as very small ^{1}H NMR chemical shifts (Figure 6) over the temperature range from 30 to −45 °C. It is interesting to note that coupling constants of $J = -36$ cm^{-1} and $J = -42$ cm^{-1} have also been reported for the μ-hydroxo complexes with BF_4^- and ClO_4^- counterions.[14]

Computational Analysis. To try to understand the origin of the spin-state ordering, a series of computational studies on **1**·X with several counteranions were performed. Each core has quartet and sextet spin states that are very close in energy, whereby the relative ordering is dependent on the environmental perturbations as well as the nature of ligands and substituents.

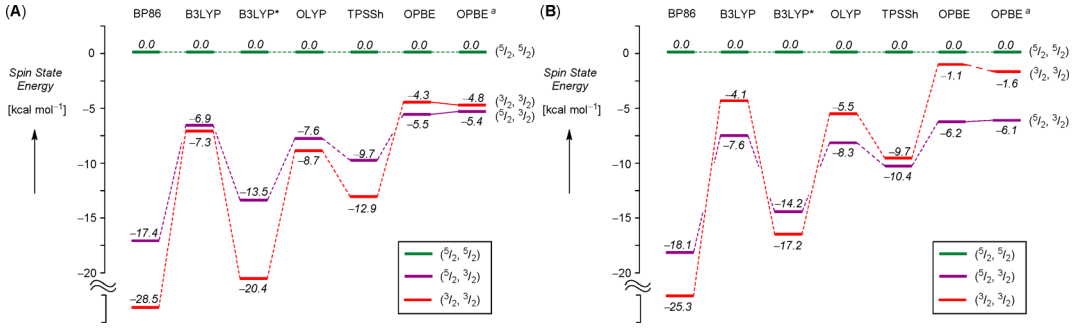

Figure 8. Relative spin-state energies of ($^5/_2$, $^5/_2$), ($^5/_2$, $^3/_2$), and ($^3/_2$, $^3/_2$) states of structure **1b** as calculated with various DFT/BS2 methods in Gaussian. Calculations done with basis set BS3 labeled with superscript a. (a) ΔE values relative to the $S = ({}^5/_2, {}^5/_2)$ state. (b) ΔE+ZPE values relative to the $S = ({}^5/_2, {}^5/_2)$ state.

DOI: 10.1021/ic502803b
Inorg. Chem. 2015, 54, 1919−1930

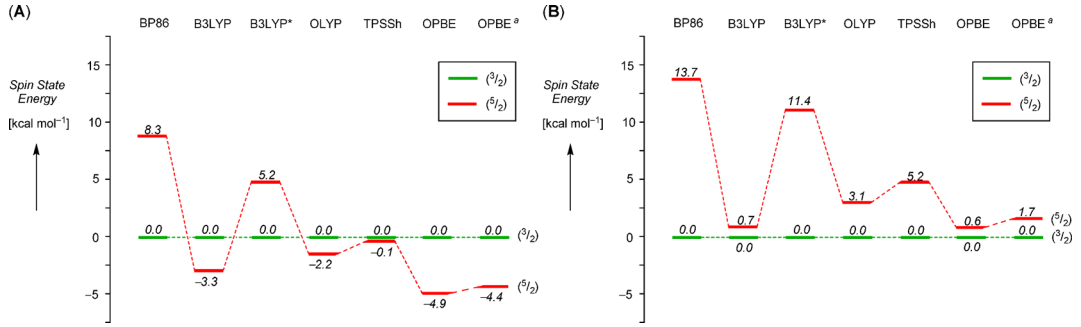

Figure 9. Quartet/sextet spin-state energies for (A) individual core I and (B) core II. All energies are relative to the quartet spin state in kcal mol^{-1}. A negative value implies an $S = {}^5/_2$ ground state.

This has analogy to enzymatic systems, and, for instance, in the resting state of cytochrome P450; that is, in the water-bound iron(III) heme cysteinate complex, the ground state is a doublet spin state,[36] but upon release of the water molecule the spin-state ordering changes, and the sextet spin state becomes the ground state.[37] In synthetic model complexes, such as cyanide ligated iron(II)tetraphenylporphyrin, a rise in the temperature leads to a spin crossover from low-spin to high-spin.[38] For $[(py)_2Fe^{III}(OEPO)]$ (OEPO = octaethyloxophlorin, py = pyridine), the iron spin state is observed to be high-spin in solid which, however, changes to a low-spin when dissolved in pyridine.[39] Moreover, many cases have been reported on rate enhancements of oxygen atom transfer reactions by axially ligated metal-porphyrin complexes.[40]

In structure **1b**·I_3 there are two iron(III) centers, and both of these have three possible spin states, which could give rise to 36 possibilities of coupling the spin states on core I with core II. For instance, a spin of $S = +{}^5/_2$ on core I can couple with a spin of $+{}^5/_2$, $+{}^3/_2$, $+{}^1/_2$, $-{}^1/_2$, $-{}^3/_2$, and $-{}^5/_2$ on core II. We did not test all these combinations, but decided to focus on the ferromagnetic coupling between spin states with combinations ($^5/_2$, $^5/_2$), ($^5/_2$, $^3/_2$), ($^3/_2$, $^3/_2$), and ($^1/_2$, $^1/_2$) only, which should give some idea of the relative stabilities of the resulting spin states. It should be noted here that the experimental results point to an admixed spin state, which would require a multireference solution of the wave function. Unfortunately, our computational models are too large for those types of calculations and, therefore, we looked at pure spin states only.

Figure 8 presents the spin-state energies of the $S = (^5/_2, {}^5/_2)$, $(^5/_2, {}^3/_2)$, and $(^3/_2, {}^3/_2)$ states of structure **1b** as calculated with six different density functional methods. The $S = (^1/_2, {}^1/_2)$ states were also calculated but found to be considerably higher in energy. We find dramatic differences in spin-state ordering and relative energies between the various DFT methods. Thus, the experimental ground state of $S = (^5/_2, {}^3/_2)$ is only reproduced with the OPBE method, although with both B3LYP and OLYP the $S = (^5/_2, {}^3/_2)$ and $S = (^3/_2, {}^3/_2)$ states are close in energy within 1.0 kcal mol^{-1}. Therefore, within the error of the calculations, the B3LYP and OLYP results can be considered a good match with experiment. The BP86 and B3LYP* methods, in contrast, give large deviations from the experimentally predicted spin-state ordering and seem to be less suitable for predicting the spin-state ordering of μ-hydroxo diiron(III)-bisporphyrin complexes. To test whether the basis set has an influence on the spin-state ordering and relative energies, we ran single-point calculations using a triple-ζ quality basis set on all atoms for structure **1b**: OPBE/BS3. However, this calculation with a larger basis set only gave minor changes in relative energies and did not change the ordering with respect to OPBE/BS2.

The results in Figure 8 show that changes in the density functional method affect the spin-state ordering and relative energies dramatically. To compare our work with experimental data, zero-point energies (ZPEs), thermal corrections, and entropic and solvent corrections were also included, and each of these factors may have a different effect on the spin-state ordering and relative energies. Importantly, a frequency calculation run on crystal structure coordinates of **1b**, gave a large number of imaginary frequencies, mostly connected to vibrations in the ethyl substituents. Therefore, a partial geometry optimization with fixed cores and flexible ethyl side chains (distances, angles, and dihedral angles containing the C and H atoms of the ethyl groups) at the B3LYP/BS1 level of theory was done prior to the frequency calculation. These structures with $S = (^5/_2, {}^5/_2)$, $S = (^5/_2, {}^3/_2)$, and $S = (^3/_2, {}^3/_2)$ spin states had no imaginary frequencies. ZPE corrections stabilize the $S = (^5/_2, {}^3/_2)$ state over the maximum spin state by 0.73 kcal mol^{-1}, whereas the $S = (^3/_2, {}^3/_2)$ state is destabilized by 3.2 kcal mol^{-1}. Consequently, addition of ZPE corrections to the energies of the data reported in Figure 8 improves the comparison between experiment and theory for most methods, and now the correct spin-state ordering is reproduced with B3LYP, OLYP, TPSSh, and OPBE. Despite the fact that the energy gap between the $S = (^5/_2, {}^3/_2)$ and the $S = (^3/_2, {}^3/_2)$ states has narrowed considerably after addition of ZPE corrections, the BP86 and B3LYP* methods still predict the wrong ground state.

We then investigated the effect of the ZPE, thermal, and entropic corrections on the spin-state ordering and associated relative energies. It is found that free energy lowers the $S = (^5/_2, {}^3/_2)$ state over the $S = (^5/_2, {}^5/_2)$ state with respect to the ΔE values by 1.4 kcal mol^{-1}, while the $S = (^3/_2, {}^3/_2)$ state is stabilized over the $S = (^5/_2, {}^5/_2)$ state by 0.4 kcal mol^{-1}. This implies that at the free energy level, the experimental spin-state ordering is reproduced using the B3LYP, OLYP, and OPBE methods only.

To understand the origin of the large variation in spin-state ordering and relative energies between the various DFT methods we decided to split structure **1b** into two individual cores and calculate those separately. Thus, we took structure **1b** and separated it into two cores, whereby the bridging ethyl group was included in both cores and capped with a hydrogen atom. We initially investigated both cores with a hydroxo ligand in the distal position, and Figure 9a,b displays the spin-state ordering and relative energies of core I and core II, respectively. Thus, all DFT methods predict an $S = {}^3/_2$ ground state for core II, but the spin-state ordering for core I varies with the DFT methods. Moreover, the quartet-sextet energy splitting varies by more than 13 kcal

DOI: 10.1021/ic502803b
Inorg. Chem. 2015, 54, 1919−1930

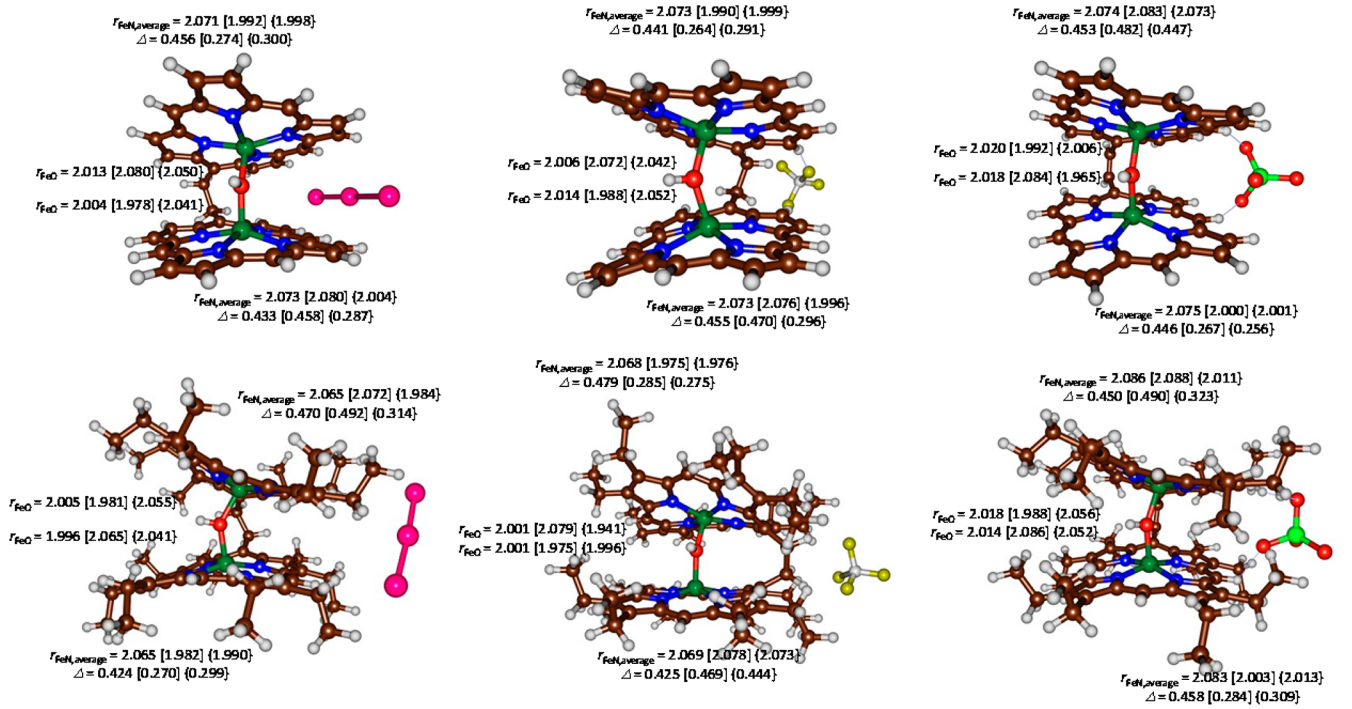

Figure 10. Optimized geometries of the $S = ({}^5/_2, {}^5/_2)$, $[S = ({}^5/_2, {}^3/_2)]$, and $\{S = ({}^3/_2, {}^3/_2)\}$ states of **1a**·X and **1b**·X with X = I_3^-, BF_4^-, or ClO_4^- at the B3LYP/BS1 level of theory in Jaguar. Bond lengths are given in angstroms, and Δ is the average deviation of the iron from the plane through the four nitrogen atoms.

mol^{-1} for each individual core, whereby the BP86 method gives a large stabilization of the quartet spin state over the sextet spin state. Hence, the overstabilization of lower spin states by pure density functionals such as BP86 therefore makes these methods unsuitable for the correct description of μ-hydroxo diiron(III)-bisporphyrin complexes. Also the reduced amount of HF exchange in the B3LYP* method overstabilizes the quartet spin states by a too large amount and therefore gives the wrong spin-state ordering of the complex. The B3LYP, OLYP, TPSSh, and OPBE methods all predict the correct spin-state ordering for each of the individual cores and give a small quartet/sextet spin-state energy gap.

A comparison of the quartet-sextet energy splitting in core I as compared to the energy difference in **1b** between the $S = ({}^5/_2, {}^3/_2)$ and $S = ({}^3/_2, {}^3/_2)$ states is a measure of the intramolecular interactions of core II with core I. In all cases, the dinuclear complex shows extra stabilization of the $S = {}^3/_2$ state on both core I and core II. On core I the quartet spin state of the isolated core with respect to the dinuclear complex is stabilized over the sextet spin state by 1.8−3.7 kcal mol^{-1} for the seven methods described in Figures 8 and 9, whereas a stabilization of 2.1−6.2 kcal mol^{-1} is found for core II. This means that the antiferromagnetic interaction between the two cores, the porphyrin ring deformation, and $\pi-\pi$ stacking interactions lead to a stabilization of the quartet spin state on each core with respect to the sextet spin state, which is independent of the density functional method and basis set. Ring deformation is known to stabilize intermediate spin states over high-spin states in iron(III) porphyrin complexes.[11,12] Indeed, in our particular system both porphyrin rings show considerable ruffling but not by the same degree, hence leading to different spin states on each iron center.

To test the effect of ZPE, thermal, and entropic corrections on the spin-state ordering of the two individual cores, we ran a partial geometry optimization at B3LYP/BS1 where we fixed the first and second coordination sphere of atoms around the iron center and reoptimized the rest. This led to a structure without imaginary frequencies and almost negligible change in ZPE for both spin states. The quartet spin state is stabilized over the sextet spin state by 0.2 and 0.1 kcal mol^{-1} for cores I and II, respectively. Subsequently, we investigated the free energy differences of these structures in the relevant spin states, and when the full combination of ZPE, thermal, and entropic corrections are included the sextet spin state is favored by 0.9 and 0.6 kcal mol^{-1} for core I and core II, respectively. This is not surprising as the entropy component contains a factor $-RT\cdot\ln(2S+1)$, which has a value of 4.4 kcal mol^{-1} for the sextet spin state and 3.4 kcal mol^{-1} for the quartet spin state at a temperature of 298 K. As our spin-state splittings are small, this extra stabilization of the free energy due to electron spin may tip the balance in favor of the high-spin state.

To further establish the environmental effects on the spin-state ordering and relative energies, we decided to include counter-anions, that is, I_3^-, BF_4^-, and ClO_4^-, into the model. We took the crystal structure coordinates of **1b**·X with X = I_3^-, BF_4^-, and ClO_4^- and did a full geometry optimization without constraints for the three relevant spin states, that is, $S = ({}^5/_2, {}^5/_2)$, $S = ({}^5/_2, {}^3/_2)$, and $S = ({}^3/_2, {}^3/_2)$, for **1a**·X and **1b**·X. The obtained structures of the complexes are shown in Figure 10. Counter ions have small and virtually insignificant effects on the optimized geometries, and, as follows from Figure 10, we find very similar structures for **1a**·X (X = I_3^-, BF_4^-, or ClO_4^-). The same trends are found for the large system with ethyl substituents attached to the porphyrin scaffold (**1b**·X). Of course, there are geometric differences between the spin states as discussed above. A geometry optimization elongates both Fe−O distances from 1.897/1.934 Å in the crystal structure to slightly over 2.0 Å. On the other hand, very little changes are found for the porphyrin groups: the average

DOI: 10.1021/ic502803b
Inorg. Chem. 2015, 54, 1919−1930

Table 3. Relative Energies of Optimized Geometries in Different Spin States of 1a·X and 1b·X Complexes[a]

	ΔE (ΔE+ZPE)	ΔE (ΔE+ZPE)	ΔE (ΔE+ZPE)	ΔE (ΔE+ZPE)	ΔE (ΔE+ZPE)
	X = I_3^-	X = BF_4^-		X = ClO_4^-	
	B3LYP/BS1	B3LYP/BS1	OPBE/BS1	B3LYP/BS1	OPBE/BS1
1a·X					
$S = (^5/_2, ^5/_2)$	0.00 (0.00)	0.00 (0.00)		0.00 (0.00)	
$S = (^5/_2, ^3/_2)$	−6.07 (−5.23)	−4.99 (−3.88)		−5.83 (−4.70)	
$S = (^3/_2, ^3/_2)$	−9.87 (−7.79)	−9.83 (−7.78)			
1b·X					
$S = (^5/_2, ^5/_2)$	0.00 (0.00)	0.00 (0.00)	0.00 (0.00)	0.00 (0.00)	0.00 (0.00)
$S = (^5/_2, ^3/_2)$	−5.90 (−4.84)	−6.11 (−5.16)	−2.83 (−1.66)	−5.69 (−4.75)	−3.00 (−1.61)
$S = (^3/_2, ^3/_2)$	−11.08 (−8.74)		−4.62 (−2.29)	−9.12 (−7.09)	−4.29 (−1.53)

[a]Energies in kcal mol^{-1} with ZPE corrected values in parentheses.

Fe−N distances in core I/core II are 2.051/2.006 Å in the crystal structure, which are values close to those seen in Figure 10. Also the displacement of the metal from the plane through the four nitrogen atoms (defined as Δ) is virtually the same in the optimized geometries as compared to the crystal structures.

Table 3 provides relative energies of the $S = (^5/_2, ^5/_2)$, $S = (^5/_2, ^3/_2)$, and $S = (^3/_2, ^3/_2)$ optimized geometries of **1a**·X and **1b**·X (X = I_3^-, BF_4^-, or ClO_4^-) as calculated with B3LYP and OPBE. Energetically, in all cases the $S = (^3/_2, ^3/_2)$ state is the ground state followed by the $S = (^5/_2, ^3/_2)$ state and the $S = (^5/_2, ^5/_2)$ state. Only very small changes in energies are obtained when counterions are added, and no clear changes are observed, based on the nature of the counterions. The same trends are found for B3LYP and OPBE as density functional method. Clearly, in the gas phase the effect of counterions is small and does not induce changes in the spin-state ordering and relative energies. As discussed above, environmental effects can change the relative spin-state ordering, and in some cases a different electronic ground state is observed experimentally in solution than in a crystal structure.

Interestingly, the relative energies in Table 3 are similar to those reported above in Figure 10a, where we reported single-point DFT calculations on the crystal structure coordinates. However, correction for ZPE by a partial geometry optimization lowered the $S = (^5/_2, ^3/_2)$ below the $S = (^3/_2, ^3/_2)$ state, which is not seen when a full geometry optimization and frequency calculation is performed. As such, minor geometric distortions to the structure affect the spin-state ordering and electronic ground state of μ-hydroxo-bridged diiron complexes. We should note here that the relative energies can be further affected by spin−orbital coupling also.[41] It may very well be that the degree of spin−orbit coupling is affected by nearby anions, such as counteranions, which thereby changes the spin-state ordering as observed experimentally.

The data shown in Table 3 indicate that the energetic differences between the three main spin states are very small and that in the gas phase, there is a preference for an $S = (^3/_2, ^3/_2)$ spin state. As reasoned above, entropic corrections will favor higher spin states and consequently, an increase of the temperature will strongly influence the spin-state ordering. We note, however, that in the optimized geometries, the counteranion is aligned with the dipole moment vector of the diiron porphyrin complex as expected for an ion-dipole interaction. The change in spin state upon addition of counterions observed experimentally, may, therefore, result from a combination of factors, of which some are not included in the computational models. The hydrogen bonding interactions of solvent molecules to the bridging μ-hydroxo group may play a key role in establishing the electronic ground state, and this was not considered in the models used here. Furthermore, an induced electric field was shown to strongly affect the spin-state ordering, which may have an effect in the systems studied here.[42] Finally, spin−orbit coupling can influence the small energy differences and change the relative ordering between the various spin states.

It would be interesting to compare the spin states of μ-hydroxo diiron(III)bisporphyrins obtained from experiment and theory. Experimentally, **1b**·I_3 is assigned to have nearly high-spin and admixed-intermediate spins of iron in cores I and II, respectively, which is also reproduced in theory using the crystal structure coordinates of the molecule utilizing a variety of hybrid and nonhybrid exchange correlation functionals. However, two admixed-intermediate spins of iron are experimentally observed in **1b**·BF_4, **1b**·PF_6, and **1b**·SbF_6. In fact, the contributions of intermediate spin states were increased substantially in **1b**·PF_6 and **1b**·SbF_6 reported here. Energetically, the $S = (^3/_2, ^3/_2)$ state is the ground state followed by the $S = (^5/_2, ^3/_2)$ state and then the $S = (^5/_2, ^5/_2)$ state for most of the complexes described here. It is interesting to note here that two Fe centers in **1b**·ClO_4, which are found to be high-spin ($S = ^5/_2$) in the solid state, convert to the intermediate-spin ($S = ^3/_2$) in solution. One probable reason could be the breaking of H-bonding interactions observed in the solid once it dissolved in solution. Thus, subtle change in the environment can also affect the relative spin-state ordering and in some cases a different electronic ground state. The relative energies of the spin states are also known to be affected by the extent of spin−orbital coupling, which can be influenced by the nearby counteranions. Moreover, an induced electric field can also affect spin-state ordering and relative energies therein. Thus, the different spin-state behavior of **1b**·X, as observed in the experiment, can be attributed to the properties of the counteranion X, which are also known to operate under the influence of variety of phenomena related to steric effects, charge polarization, stability of the ion-pair formations, etc., and were not considered in the computational models used here.

CONCLUSIONS

We have provided a combination of experimental and computational studies on a series of hydroxo-bridged diiron(III)-bisporphyrin complexes with particular focus on the spin-state ordering. Experimental work shows a strong variation in electronic ground state for **1b**·X (X = I_3^-, BF_4^-, ClO_4^-, PF_6^-, SbF_6^-). Crystallographic studies show considerable ruffling of both porphyrin rings by unequal amounts, and the doming and structural features are characteristic of a spin state. ^{1}H NMR and

DOI: 10.1021/ic502803b
Inorg. Chem. 2015, 54, 1919−1930

Mössbauer studies confirmed this assignment. Finally, an extensive computational study was performed on various diiron(III)bisporphyrin complexes with a range of DFT methods, which established a variety of factors that affect spin-state ordering and relative energies in μ-hydroxo bridged diiron(III)bisporphyrin complexes. The latter highlights the small energy gap between the $S = ({}^3/_2, {}^3/_2)$ and $S = ({}^5/_2, {}^3/_2)$ spin states and how their ordering can interchange through external perturbations.

■ ASSOCIATED CONTENT

Supporting Information

Crystal data and data collection parameters. X-ray crystallographic details in CIF format. Computational details as well as tables with group spin densities, charges, and relative energies. The Gaussian reference in full. This material is available free of charge via the Internet at http://pubs.acs.org.

■ AUTHOR INFORMATION

Corresponding Authors

*E-mail: sam.devisser@manchester.ac.uk. (S.P.d.V.)
*E-mail: peter.comba@aci.uni-heidelberg.de. (P.C.)
*E-mail: sprath@iitk.ac.in. (S.P.R.)

Notes

The authors declare no competing financial interest.

■ ACKNOWLEDGMENTS

M.A.S. thanks the Petroleum Technology Development Fund for a studentship. The National Service of Computational Chemistry Software is thanked for providing valuable central processing unit time. The EU-COST Network CM1003 "Biological Oxidation Reactions" is thanked for funding for two short-term scientific missions to Heidelberg of M.A.S. and S.d.V. P.C. and B.M. are grateful for financial support from the German Science Foundation and the University of Heidelberg. S.P.R. thanks Science and Engineering Research Board, New Delhi, and CSIR, India, for financial support. D.S. and D.S. thank the University Grants Commission (India), while S.P.R. thanks the Alexander von Humboldt Foundation for awarding a Fellowship.

■ REFERENCES

(1) See, for example, (a) Wilkins, P. C.; Wilkins, R. G. *Coord. Chem. Rev.* **1987**, *79*, 195−214. (b) Stenkamp, R. E. *Chem. Rev.* **1994**, *94*, 715−726.

(2) See, for example, (a) Nordlund, P.; Reichard, P. *Annu. Rev. Biochem.* **2006**, *75*, 681−706. (b) Tomter, A. B.; Zoppellaro, G.; Andersen, N. H.; Hersleth, H.-P.; Hammerstad, M.; Røhr, Å. K.; Sandvik, G. K.; Strand, K. R.; Nilsson, G. E.; Bell, C. B., III; Barra, A.-L.; Blasco, E.; Le Pape, L.; Solomon, E. I.; Andersson, K. K. *Coord. Chem. Rev.* **2013**, *257*, 3−26. (c) Krebs, C.; Dassama, L. M. K.; Matthews, M. L.; Jiang, W.; Price, J. C.; Korboukh, V.; Li, N.; Bollinger, J. M., Jr *Coord. Chem. Rev.* **2013**, *257*, 234−243.

(3) Moënne-Loccoz, P.; Krebs, C.; Herlihy, K.; Edmondson, D. E.; Theil, E. C.; Huynh, B. H.; Loehr, T. M. *Biochemistry* **1999**, *38*, 5290−5295.

(4) See, e.g., (a) Murray, L. J.; Lippard, S. J. *Acc. Chem. Res.* **2007**, *40*, 466−474. (b) Balasubramanian, R.; Rosenzweig, A. C. *Acc. Chem. Res.* **2007**, *40*, 573−580.

(5) (a) Shanklin, J.; Somerville, C. *Proc. Natl. Acad. Sci. U.S.A.* **1991**, *88*, 2510−2514. (b) Fox, B. G.; Lyle, K. S.; Rogge, C. E. *Acc. Chem. Res.* **2004**, *37*, 421−429.

(6) (a) Ferguson-Miller, S.; Babcock, G. T. *Chem. Rev.* **1996**, *96*, 2889−2907. (b) Collman, J. P.; Boulatov, R.; Sunderland, C. J.; Fu, L. *Chem. Rev.* **2004**, *104*, 561−588. (c) Belevich, I.; Verkhovsky, M. I.; Wikström, M. *Nature* **2006**, *440*, 829−832. (d) Siegbahn, P. E. M.; Blomberg, M. R. A. *J. Phys. Chem. A* **2008**, *112*, 12772−12780.

(7) (a) Chufán, E. E.; Puiu, S. C.; Karlin, K. D. *Acc. Chem. Res.* **2007**, *40*, 563−572. (b) Itoh, S. *Curr. Opin. Chem. Biol.* **2006**, *10*, 115−122. (c) Quintanar, L.; Stoj, C.; Taylor, A. B.; Hart, P. J.; Kosman, D. J.; Solomon, E. I. *Acc. Chem. Res.* **2007**, *40*, 445−452.

(8) (a) Rosenzweig, A. C.; Lippard, S. J. *Acc. Chem. Res.* **1994**, *27*, 229−236. (b) Dassama, L. M. K.; Silakov, A.; Krest, C. M.; Calixto, J. C.; Krebs, C.; Bollinger, J. M., Jr.; Green, M. T. *J. Am. Chem. Soc.* **2013**, *135*, 16758−16761. (c) Korendovych, I. V.; Kryatov, S. V.; Rybak-Akimova, E. V. *Acc. Chem. Res.* **2007**, *40*, 510−521.

(9) (a) Shaik, S.; Filatov, M.; Schröder, D.; Schwarz, H. *Chem.—Eur. J.* **1998**, *4*, 193−199. (b) Shaik, S.; de Visser, S. P.; Ogliaro, F.; Schwarz, H.; Schröder, D. *Curr. Opin. Chem. Biol.* **2002**, *6*, 556−567.

(10) (a) Green, M. T. *J. Am. Chem. Soc.* **1999**, *121*, 7939−7940. (b) *Iron-Containing Enzymes: Versatile Catalysts of Hydroxylation Reactions in Nature;* de Visser, S. P., Kumar, D., Eds.; Royal Society of Chemistry Publishing: Cambridge, U.K., 2011.

(11) (a) Bhowmik, S.; Ghosh, S. K.; Layek, S.; Verma, H. C.; Rath, S. P. *Chem.—Eur. J.* **2012**, *18*, 13025−13037. (b) Ghosh, S. K.; Rath, S. P. *J. Am. Chem. Soc.* **2010**, *132*, 17983−17985.

(12) Ghosh, S. K.; Bhowmik, S.; Sil, D.; Rath, S. P. *Chem.—Eur. J.* **2013**, *19*, 17846−17859.

(13) (a) Kitchen, J. A.; White, N. G.; Jameson, G. N. L.; Tallon, J. L.; Brooker, S. *Inorg. Chem.* **2011**, *50*, 4586−4597. (b) Kitchen, J. A.; Brooker, S. *Coord. Chem. Rev.* **2008**, *252*, 2072−2092. (c) Nihei, M.; Shiga, T.; Maeda, Y.; Oshio, H. *Coord. Chem. Rev.* **2007**, *251*, 2606−2621. (d) Yamada, M.; Hagiwara, H.; Torigoe, H.; Matsumoto, N.; Kojima, M.; Dahan, F.; Tuchagues, J.-P.; Re, N.; Iijima, S. *Chem.—Eur. J.* **2006**, *12*, 4536−4549. (e) Gütlich, P.; Hauser, A.; Spiering, H. *Angew. Chem., Int. Ed. Engl.* **1994**, *33*, 2024−2054.

(14) (a) Ghosh, S. K.; Patra, R.; Rath, S. P. *Inorg. Chem.* **2008**, *47*, 10196−10198. (b) Ghosh, S. K.; Patra, R.; Rath, S. P. *Inorg. Chem.* **2010**, *49*, 3449−3460. (c) Ghosh, S. K.; Patra, R.; Rath, S. P. *Inorg. Chim. Acta* **2010**, *363*, 2791−2799.

(15) *SAINT+*, 6.02 ed.; Bruker AXS: Madison, WI, 1999.

(16) Sheldrick, G. M. *SADABS* 2.0; University of Göttingen: Göttingen, Germany, 2000.

(17) Sheldrick, G. M. *SHELXL-2014: Program for Crystal Structure Refinement*; University of Göttingen: Göttingen, Germany, 2014.

(18) Frisch, M. J. et al. *Gaussian 09,* Revision D.01; Gaussian, Inc.: Wallingford, CT, 2004.

(19) (a) Becke, A. D. *J. Chem. Phys.* **1993**, *98*, 5648−5652. (b) Lee, C.; Yang, W.; Parr, R. G. *Phys. Rev. B* **1988**, *37*, 785−789.

(20) Reiher, M.; Salomon, O.; Hess, B. A. *Theor. Chem. Acc.* **2001**, *107*, 48−55.

(21) (a) Becke, A. D. *Phys. Rev. A* **1988**, *38*, 3098−3100. (b) Perdew, J. P. *Phys. Rev. B* **1986**, *33*, 8822−8824.

(22) (a) Handy, N. C.; Cohen, A. J. *Mol. Phys.* **2001**, *99*, 403−412. (b) Hoe, W.-M.; Cohen, A.; Handy, N. C. *Chem. Phys. Lett.* **2001**, *341*, 319−328.

(23) Perdew, J. P.; Burke, K.; Ernzerhof, M. *Phys. Rev. Lett.* **1996**, *77*, 3865−3868.

(24) Tao, J. M.; Perdew, J. P.; Staroverov, V. N.; Scuseria, G. E. *Phys. Rev. Lett.* **2003**, *91*, 146401.

(25) (a) Hay, P. J.; Wadt, W. R. *J. Chem. Phys.* **1985**, *82*, 270−283. (b) Hehre, W. J.; Ditchfield, K.; Pople, J. A. *J. Chem. Phys.* **1972**, *56*, 2257−2261.

(26) Schaefer, A.; Huber, C.; Ahlrichs, R. *J. Chem. Phys.* **1994**, *100*, 5829−5835.

(27) *Jaguar* 7.8; Schrödinger LLC: New York, 2010.

(28) (a) Weiss, R.; Gold, A.; Terner, J. *Chem. Rev.* **2006**, *106*, 2550−2579. (b) Nakamura, M.; Ohgo, Y.; Ikezaki, A. Electronic and Magnetic Structures of Iron Porphyrin Complexes. In *Handbook of Porphyrin Science;* Kadish, K. M, Smith, K. M., Guilard, R., Eds.; World Scientific: Singapore, 2010; pp 1−146. (c) Reed, C. A.; Mashiko, T.; Bentley, S. P.; Kastner, M. E.; Scheidt, W. R.; Spartalian, K.; Lang, G. *J. Am. Chem. Soc.* **1979**, *101*, 2948.

DOI: 10.1021/ic502803b
Inorg. Chem. 2015, 54, 1919−1930

(29) (a) Scheidt, W. R.; Cheng, B.; Safo, M. K.; Cukiernik, F.; Marchon, J.-C.; Debrunner, P. G. *J. Am. Chem. Soc.* **1992**, *114*, 4420−4421. (b) Ling, Y.; Zhang, Y. *J. Am. Chem. Soc.* **2009**, *131*, 6386−6388.
(30) Evans, D. R.; Mathur, R. S.; Heerwegh, K.; Reed, C. A.; Xie, Z. *Angew. Chem., Int. Ed. Engl.* **1997**, *36*, 1335−1337.
(31) (a) Bhowmik, S.; Dey, S.; Sahoo, D.; Rath, S. P. *Chem.—Eur. J.* **2013**, *19*, 13732−13744. (b) Bhowmik, S.; Sil, D.; Patra, R.; Rath, S. P. *J. Chem. Sci.* **2011**, *123*, 827−837. (c) Bhowmik, S.; Ghosh, S. K.; Rath, S. P. *Chem. Commun.* **2011**, *47*, 4790−4792. (d) Sil, D.; Khan, F. S. T.; Rath, S. P. *Inorg. Chem.* **2014**, *53*, 11925−11936.
(32) Nakamura, K.; Ikezaki, A.; Ohgo, Y.; Ikeue, T.; Neya, S.; Nakamura, M. *Inorg. Chem.* **2008**, *47*, 10299−10307.
(33) O'Connor, C. J. *Prog. Inorg. Chem.* **1982**, *29*, 203−283.
(34) Kahn, O. *Molecular Magnetism;* VCH Publishers: Weinheim, Germany, 1993; pp 2−4.
(35) (a) Schünemann, V.; Gerdan, M.; Trautwein, A. X.; Haoudi, N.; Mandon, D.; Fischer, J.; Weiss, R.; Tabard, A.; Guilard, R. *Angew. Chem., Int. Ed. Engl.* **1999**, *38*, 3181−3183. (b) Weiss, R.; Fischer, J.; Bulach, V.; Schünemann, V.; Gerdan, M.; Trautwein, A. X.; Shelnutt, J. A.; Gros, C. P.; Tabard, A.; Guilard, R. *Inorg. Chim. Acta* **2002**, *337*, 223−236.
(36) Thomann, H.; Bernardo, M.; Goldfarb, D.; Kroneck, P. M. H.; Ullrich, V. *J. Am. Chem. Soc.* **1995**, *117*, 8243−8251.
(37) Auclair, K.; Moënne-Loccoz, P.; Ortiz de Montellano, P. R. *J. Am. Chem. Soc.* **2001**, *123*, 4877−4885.
(38) Li, J.; Lord, R. L.; Noll, B. C.; Baik, M.-H.; Schulz, C. E.; Scheidt, W. R. *Angew. Chem., Int. Ed.* **2008**, *47*, 10144−10146.
(39) Rath, S. P.; Olmstead, M. M.; Balch, A. L. *Inorg. Chem.* **2006**, *45*, 6083−6093.
(40) See, e.g., (a) de Visser, S. P.; Ogliaro, F.; Shaik, S. *Angew. Chem., Int. Ed.* **2002**, *41*, 1947−1951. (b) Nam, W.; Ryu, Y. O.; Song, W. J. *J. Biol. Inorg. Chem.* **2004**, *9*, 654−660. (c) Kumar, D.; de Visser, S. P.; Sharma, P. K.; Derat, E.; Shaik, S. *J. Biol. Inorg. Chem.* **2005**, *10*, 181−189. (d) Song, W. J.; Ryu, Y. O.; Song, R.; Nam, W. *J. Biol. Inorg. Chem.* **2005**, *10*, 294−304. (e) de Visser, S. P. *J. Biol. Inorg. Chem.* **2006**, *11*, 168−178. (f) de Visser, S. P.; Tahsini, L.; Nam, W. *Chem.—Eur. J.* **2009**, *15*, 5577−5587. (g) Hessenauer-Ilicheva, N.; Franke, A.; Meyer, D.; Woggon, W.-D.; van Eldik, R. *Chem.—Eur. J.* **2009**, *15*, 2941−2959. (h) Prokop, K. A.; de Visser, S. P.; Goldberg, D. P. *Angew. Chem., Int. Ed.* **2010**, *49*, 5091−5095. (i) Takahashi, A.; Yamaki, D.; Ikemura, K.; Kurahashi, T.; Ogura, T.; Hada, M.; Fujii, H. *Inorg. Chem.* **2012**, *51*, 7296−7305. (j) Kumar, D.; Sastry, G. N.; de Visser, S. P. *Chem.—Eur. J.* **2011**, *17*, 6196−6205.
(41) (a) Gupta, A.; Gupta, G. P. *J. Phys.: Condens. Matter* **1994**, *6*, 11071−11080. (b) Hagen, W. R.; van den Berg, W. A. M.; van Dongen, W. M. A. M.; Reijerse, E. J.; van Kan, P. J. M. *J. Chem. Soc. Farad. Trans.* **1998**, *94*, 2969−2973.
(42) (a) Shaik, S.; de Visser, S. P.; Kumar, D. *J. Am. Chem. Soc.* **2004**, *126*, 11746−11749. (b) de Visser, S. P. *J. Phys. Chem. A* **2005**, *109*, 11050−11057.

DOI: 10.1021/ic502803b
Inorg. Chem. 2015, 54, 1919−1930